Probabilistic Engineering Mechanics 59 (2020) 103016

Contents lists available at ScienceDirect

Probabilistic Engineering Mechanics

journal homepage: www.elsevier.com/locate/probengmech

Simulation of wind velocity time histories on long span structures modeled as non-Gaussian stochastic waves

Haijun Zhou [a], George Deodatis [b,*], Michael Shields [c], Brett Benowitz [b]

[a] Institute of Urban Smart Transportation & Safety Maintenance, Shenzhen, China
[b] Department of Civil Engineering & Engineering Mechanics, Columbia University, NY, USA
[c] Department of Civil Engineering, Johns Hopkins University, Baltimore, USA

ARTICLE INFO

Keywords:
Spectral representation method
Non-Gaussian stochastic wave
Frequency–wavenumber spectrum
Translation process
Fast Fourier Transform
Simulation of wind velocities

ABSTRACT

A methodology is proposed for efficient and accurate modeling and simulation of correlated non-Gaussian wind velocity time histories along long-span structures at an arbitrarily large number of points. Currently, the most common approach is to model wind velocities as discrete components of a stochastic vector process, characterized by a Cross-Spectral Density Matrix (CSDM). To generate sample functions of the vector process, the Spectral Representation Method is one of the most commonly used, involving a Cholesky decomposition of the CSDM. However, it is a well-documented problem that as the length of the structure – and consequently the size of the vector process – increases, this Cholesky decomposition breaks down numerically. This paper extends a methodology introduced by the second and fourth authors to model wind velocities as a Gaussian stochastic wave (continuous in both space and time) by considering the stochastic wave to be non-Gaussian. The non-Gaussian wave is characterized by its frequency–wavenumber (FK) spectrum and marginal probability density function (PDF). This allows the non-Gaussian wind velocities to be modeled at a virtually infinite number of points along the length of the structure. The compatibility of the FK spectrum and marginal PDF according to translation process theory is secured using an extension of the Iterative Translation Approximation Method introduced by the second and third authors, where the underlying Gaussian FK spectrum is upgraded iteratively using the directly computed (through translation process theory) non-Gaussian FK spectrum. After a small number of computationally extremely efficient iterations, the underlying Gaussian FK spectrum is established and generation of non-Gaussian sample functions of the stochastic wave is straightforward without the need of iterations. Numerical examples are provided demonstrating that the simulated non-Gaussian wave samples exhibit the desired spectral and marginal PDF characteristics.

1. Introduction

Several methods are available today to solve problems in engineering mechanics involving uncertain quantities described by stochastic processes, fields or waves. Among them, Monte Carlo simulation appears to be the only universal method that can provide accurate solutions for problems in stochastic mechanics involving strong nonlinearities, system stochasticity, stochastic stability, large variations of uncertain system parameters, etc. One of the most important steps of the Monte Carlo simulation methodology is the generation of sample functions of the stochastic processes, fields or waves involved in the problem at hand. Among the various methods currently available to generate such sample functions, the Spectral Representation Method (SRM) [1] is one of the most widely used today.

Wind is the governing load on long span bridges and exhibits a high degree of uncertainty [2]. When performing a Monte Carlo simulation analysis of a long-span bridge subjected to wind loads, the standard approach today is to model the wind velocity time histories as components of a stochastic vector process (or equivalently a multivariate stochastic process), characterized by its Cross-Spectral Density Matrix (CSDM). When the SRM is used to generate sample functions of this stochastic vector process, its CSDM has to be decomposed using Cholesky [3] or modal [4–6] decomposition. However, for both modal and Cholesky type decompositions, there is a serious problem when the number of components in the vector process becomes large. These decompositions break down numerically because neighboring points on the bridge have wind velocity time histories that are highly correlated to each other, and the CSDM gets increasingly close to becoming singular. To address this problem, some research efforts have focused on developing approximate techniques to facilitate this decomposition (e.g. [7–10]). However, these methods remain quite expensive computationally, involve different degrees of approximation,

* Corresponding author.
E-mail addresses: haijun@szu.edu.cn (H. Zhou), deodatis@columbia.edu (G. Deodatis), michael.shields@jhu.edu (M. Shields).

https://doi.org/10.1016/j.probengmech.2020.103016
Received 14 January 2020; Accepted 17 January 2020
Available online 20 January 2020

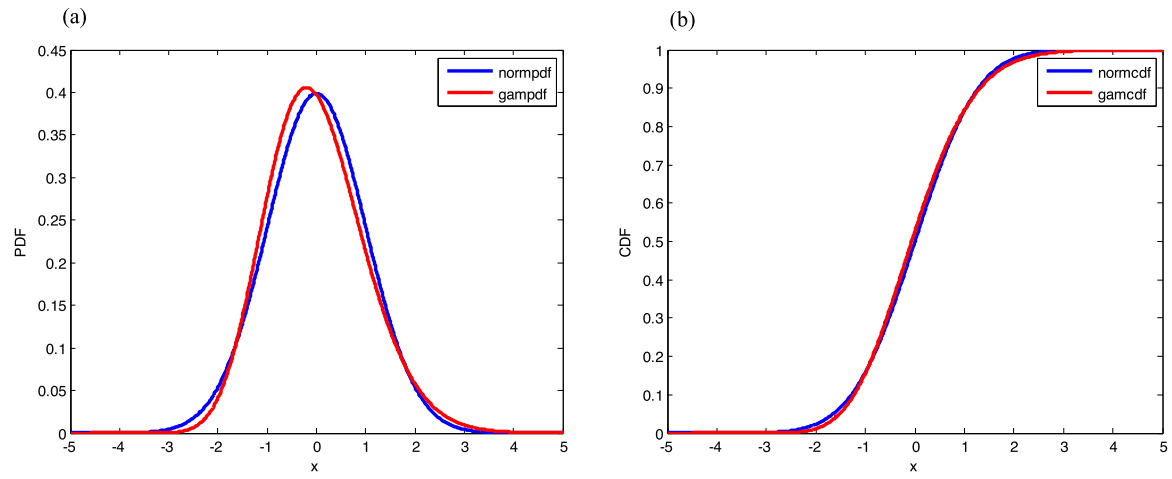

Fig. 1. Gamma distribution used in the numerical examples compared to the Gaussian distribution with same mean and standard deviation: (a) PDF's, (b) CDF's.

and eventually break down when the number of components in the vector process becomes too large.

Recently, Benowitz and Deodatis [11,12] proposed an alternative formulation that can simulate wind velocity time histories at an arbitrarily large number of spatial locations without any approximating assumption or loss of accuracy. The proposed formulation models wind velocities as a continuous stochastic "wave" in the space–time domain, rather than as a discrete stochastic vector process in space and continuous only in time. This idea was then extended for conditional interpolation for unevenly spaced locations [13], non-stationary waves [14], and non-homogeneous waves in two space dimensions [15]. All of these works [11–15], however, considered the stochastic waves modeling wind velocities to be Gaussian. In this paper, the formulation introduced by Benowitz and Deodatis [11,12] for Gaussian stochastic waves is extended to non-Gaussian stochastic waves using translation process theory [16,17] as wind velocities can exhibit non-Gaussian characteristics.

2. Spectral representation method for simulation of Gaussian stochastic waves

When generating samples of a Gaussian stochastic wave $u(t,x)$ according to its frequency–wavenumber spectrum (FKS) $S_G(\omega,\kappa)$, the Spectral Representation Method (SRM) takes the following form [12]:

$$u(t,x) = \sqrt{2}\sum_{l=1}^{N_\kappa}\sum_{m=1}^{N_\omega}\sum_{I_\omega=\pm 1}\sqrt{2S_G\left(I_\omega\omega_m,\kappa_l\right)\Delta\omega\Delta\kappa}\,\cos\left[I_\omega\omega_m t+\kappa_l x+\phi_{ml}^{I_\omega}\right] \tag{1}$$

where:

$$\omega_m = m\Delta\omega\,;\ \Delta\omega = \frac{\omega_u}{N_\omega}\,;\ \kappa_l = l\Delta\kappa\,;\ \Delta\kappa = \frac{\kappa_u}{N_\kappa} \tag{2}$$

In order to take advantage of the Fast Fourier Transform (FFT) technique, Eq. (1) is rearranged as follows [12]:

$$u(t,x) = \mathrm{Re}\left[\sum_{l=0}^{N_k-1}\sum_{m=0}^{N_\omega-1}\left\{B_{lm}^{(1)}\exp\left[i\omega_m t+i\kappa_l x\right]\ +\ B_{lm}^{(2)}\exp\left[-i\omega_m t+i\kappa_l x\right]\right\}\right] \tag{3}$$

where i is the imaginary unit, $\mathrm{Re}[\cdot]$ denotes the real part, and:

$$B_{lm}^{(n)} = 2\sqrt{S\left(\omega_m,\kappa_l\right)\Delta\omega\,\Delta\kappa}\cdot\exp[i\phi_{lm}^{(n)}] \tag{4}$$

Using a pseudo-notation for the FFT, Eq. (3) can be re-written as a series of FFTs [12]:

$$u(t,x) = \mathrm{Re}\left\{FFT_\kappa\left[FFT_\omega\left(\mathbf{B}^{(1)}\right)\right] + FFT_\kappa\left[IFFT_\omega\left(\mathbf{B}^{(2)}\right)\right]\right\} \tag{5}$$

where $FFT(\cdot)$ and $IFFT(\cdot)$ denote the FFT and the Inverse FFT, respectively, and subscripts ω and κ indicate along which dimension the (I)FFT is computed.

3. Translation process theory for stochastic waves

Let $u(t,x)$ be a stationary and homogeneous Gaussian stochastic wave with zero mean, standard deviation σ, and autocorrelation function (ACF) $R_G(\tau,\xi)$. This Gaussian wave can then be mapped to a non-Gaussian one $u_{NG}(t,x)$ with prescribed marginal cumulative distribution function (CDF) $F_{NG}(\cdot)$, through the following non-linear transformation known as "translation" [16,17]:

$$u_{NG}(t,x) = F_{NG}^{-1}\left[F_G\left\{u(t,x)\right\}\right] \tag{6}$$

where $F_G(\cdot)$ is the Gaussian CDF. This transformation from Gaussian to non-Gaussian is always possible in a "forward" fashion. The Gaussian ACF $R_G(\tau,\xi)$ is transformed to the corresponding non-Gaussian ACF $R_{NG}(\tau,\xi)$ using the following equation proposed by Grigoriu [16,17]:

$$R_{NG}(\tau,\xi) = \int_{-\infty}^{\infty}\int_{-\infty}^{\infty}F_{NG}^{-1}\left\{F_G\left[x_1\right]\right\}\cdot F_{NG}^{-1}\left\{F_G\left[x_2\right]\right\} \times\boldsymbol{\Phi}\left\{x_1,x_2;\rho(\tau,\xi)\right\}dx_1dx_2 \tag{7}$$

where $\boldsymbol{\Phi}\left\{x_1,x_2;\rho(\tau,\xi)\right\}$ is the joint Gaussian probability density:

$$\boldsymbol{\Phi}\left\{x_1,x_2;\rho(\tau,\xi)\right\} = \frac{1}{2\pi\sigma^2\sqrt{1-\rho^2(\tau,\xi)}}\exp\left(\frac{x_1^2+x_2^2-2\rho(\tau,\xi)x_1x_2}{2\sigma^2\left(1-\rho^2(\tau,\xi)\right)}\right) \tag{8}$$

and $\rho(\tau,\xi)$ is the normalized Gaussian correlation function:

$$\rho(\tau,\xi) = \frac{R_G(\tau,\xi)}{\sigma^2} \tag{9}$$

4. Proposed methodology for simulation of non-Gaussian stochastic waves

The methodology in this section is an extension of the Iterative Translation Approximation Method introduced by Shields, Deodatis and Bocchini [18].

4.1. Define target non-Gaussian CDF & FKS, and initialize underlying Gaussian FKS

The non-Gaussian stochastic wave is defined by its marginal non-Gaussian CDF $F_{NG}(\cdot)$ and its non-Gaussian FKS $S_{NG}^T(\omega,\kappa)$. According to translation process theory, $F_{NG}(\cdot)$ and $S_{NG}^T(\omega,\kappa)$ are in general incompatible if defined arbitrarily and independently. The first step in

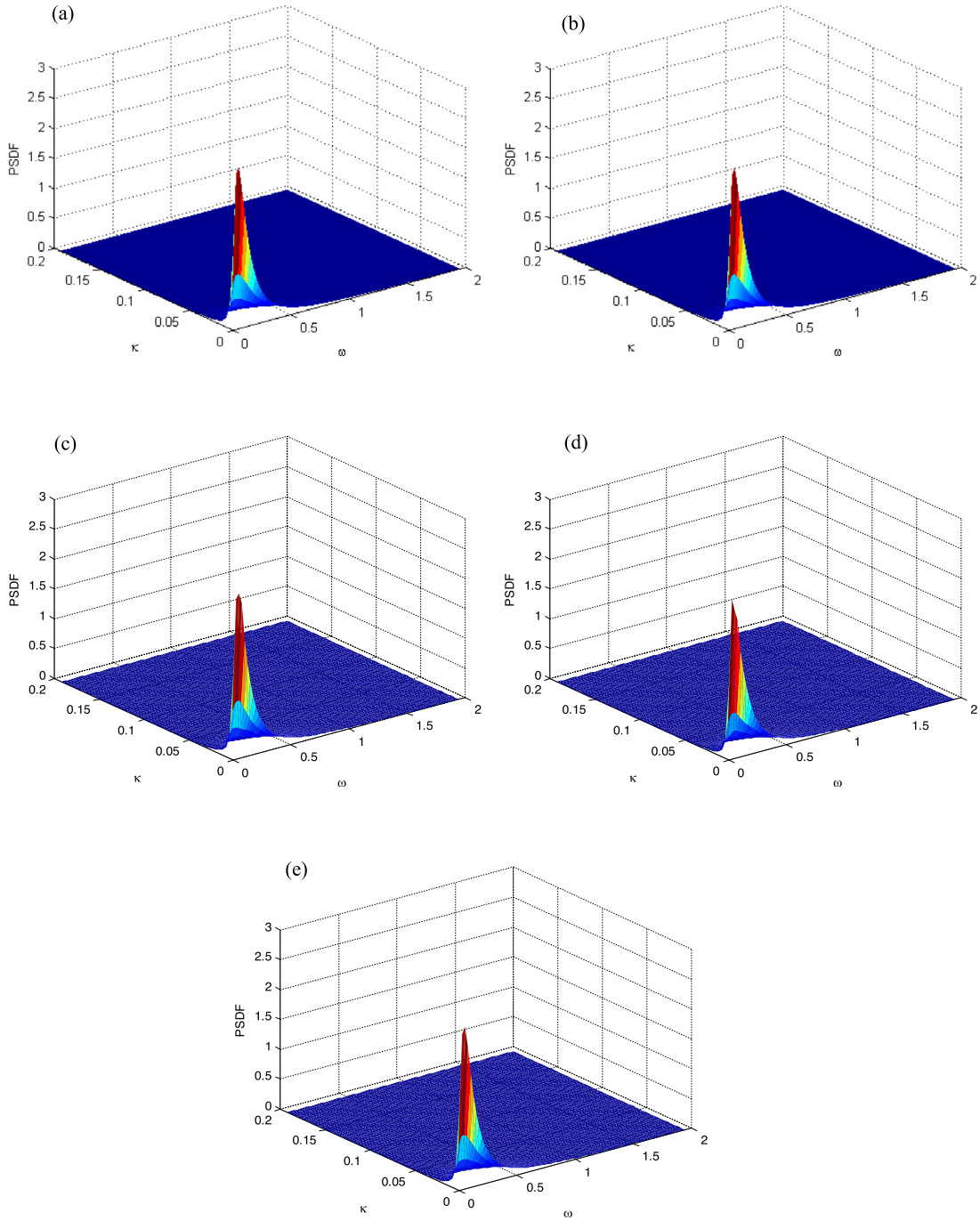

Fig. 2. (a) Gaussian FKS $S_G(\omega,\kappa)$ at the end of the iterative process, (b) Non-Gaussian FKS $S_{NG}(\omega,\kappa)$ at the end of the iterative process, (c) Ensemble FKS of 5000 generated Gaussian samples, (d) Ensemble FKS of 5000 generated non-Gaussian samples, (e) Prescribed target FKS $S^T_{NG}(\omega,\kappa)$.

the proposed iterative methodology is to provide an initial guess for the underlying Gaussian FKS $S_G(\omega,\kappa)$. Here, the initial guess for $S_G(\omega,\kappa)$ is the prescribed non-Gaussian FKS $S^T_{NG}(\omega,\kappa)$ (which is almost always an excellent choice for the initial guess).

4.2. Determining non-Gaussian FKS from Gaussian FKS at iteration (i)

Given the Gaussian FKS $S^{(i)}_G(\omega,\kappa)$ at iteration (i), the corresponding Gaussian ACF $R^{(i)}_G(\tau,\xi)$ can be computed using the Wiener–Khintchine transform:

$$R^{(i)}_G(\tau,\xi)=\int_{-\infty}^{\infty}\int_{-\infty}^{\infty}S^{(i)}_G(\omega,\kappa)\,e^{i(\omega\tau+\kappa\xi)}d\omega\,d\kappa \tag{10}$$

The Gaussian normalized correlation function $\rho^{(i)}_G(\tau,\xi)$ at iteration (i) is then computed as:

$$\rho^{(i)}_G(\tau,\xi)=\frac{R^{(i)}_G(\tau,\xi)}{\sigma^2_G} \tag{11}$$

where σ^2_G is the variance of the (zero mean) underlying Gaussian wave. The non-Gaussian ACF $R^{(i)}_{NG}(\tau,\xi)$ is computed next, using the classic translation process non-linear mapping [16,17]:

$$R^{(i)}_{NG}(\tau,\xi)=\int_{-\infty}^{\infty}\int_{-\infty}^{\infty}F^{-1}_{NG}\left\{F_G\left[x_1\right]\right\}\cdot F^{-1}_{NG}\left\{F_G\left[x_2\right]\right\}\times\Phi\left\{x_1,x_2;\rho^{(i)}_G(\tau,\xi)\right\}dx_1dx_2 \tag{12}$$

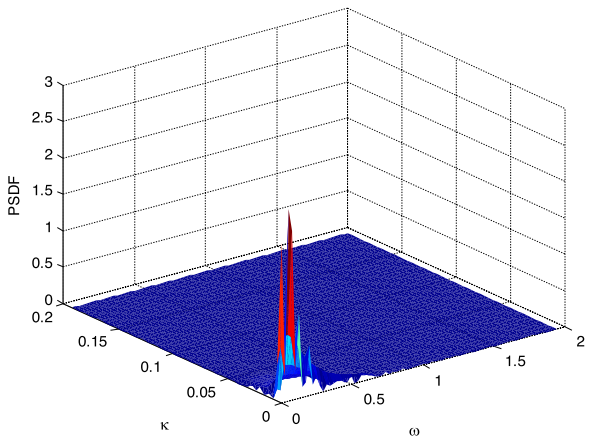

Fig. 3. FKS of one generated non-Gaussian sample function.

Finally, the corresponding non-Gaussian FKS $S_{NG}^{(i)}(\omega,\kappa)$ at iteration (i) is computed using the inverse Wiener–Khintchine transform:

$$S_{NG}^{(i)}(\omega,\kappa)=\frac{1}{(2\pi)^2}\int_{-\infty}^{\infty}\int_{-\infty}^{\infty}R_{NG}^{(i)}(\tau,\xi)\,e^{-i(\omega\tau+\kappa\xi)}d\tau d\xi \tag{13}$$

4.3. Upgrade the Gaussian FKS for iteration $(i+1)$

The underlying Gaussian FKS is upgraded for iteration $(i+1)$ using the calculated non-Gaussian FKS for iteration (i) as proposed initially by Deodatis and Micaletti [19]:

$$S_G^{(i+1)}(\omega,\kappa)=\left[\frac{S_{NG}^{T}(\omega,\kappa)}{S_{NG}^{(i)}(\omega,\kappa)}\right]^{\beta}S_G^{(i)}(\omega,\kappa) \tag{14}$$

The iterative scheme is terminated when the relative difference between the computed non-Gaussian FKS $S_{NG}^{(i+1)}(\omega,\kappa)$ and the target non-Gaussian FKS $S_{NG}^{T}(\omega,\kappa)$:

$$\epsilon_{(i+1)}=100\sqrt{\frac{\sum_{m,l}\left[S_{NG}^{(i+1)}(\omega_m,\kappa_l)-S_{NG}^{T}(\omega_m,\kappa_l)\right]^2}{\sum_{m,l}\left[S_{NG}^{T}(\omega_m,\kappa_l)\right]^2}} \tag{15}$$

stabilizes to a constant value or when further iterations are not able to lower the value of this relative difference. Because of the original incompatibility between $S_{NG}^{T}(\omega,\kappa)$ and $F_{NG}(\cdot)$, it is of course impossible for $S_{NG}^{(i+1)}(\omega,\kappa)$ to perfectly converge to $S_{NG}^{T}(\omega,\kappa)$, but it generally gets as close as possible to it, while ensuring translation-type compatibility between $S_{NG}^{(i+1)}(\omega,\kappa)$ and $F_{NG}(\cdot)$.

5. Numerical examples

A zero-mean Gamma distribution with unit standard deviation [20] is selected for the marginal probability distribution of the stochastic wave modeling wind velocities. Its PDF is given by:

$$f(x)=\frac{1}{\Gamma(k)\theta^k}\overline{x}^{k-1}e^{-\frac{\overline{x}}{\theta}} \tag{16}$$

where:

$$\theta=\frac{\sigma^2}{\overline{\mu}}\,;\ k=\frac{\overline{\mu}}{\theta}\,;\ \overline{x}=x-\overline{\mu} \tag{17}$$

Selecting the following values for parameters $\overline{\mu}$ and σ^2: $\overline{\mu}=5$, $\sigma^2=1$, leads to the following moments for the Gamma distribution: mean = 0, variance = 1, skewness = 0.4, kurtosis = 3.24. The resulting distribution is defined over the interval $[-5,\infty]$ and is plotted in Fig. 1. It is clear that its difference to the Gaussian is rather slight.

The selected target non-Gaussian power spectral density function is the Kaimal spectrum [21]:

$$S_{NG}(\omega)=\frac{1}{2}\frac{200}{2\pi}u_*^2\frac{z}{U(z)}\frac{1}{\left[1+50\frac{\omega z}{2\pi U(z)}\right]^{5/3}} \tag{18}$$

where z is the height above ground, $U(z)$ is the average wind velocity at height z, and u_* is the shear velocity defined as:

$$u_*=\frac{kU(z)}{\ln\left(z/z_0\right)} \tag{19}$$

where k is von Karman's constant ($k\cong 0.4$) and z_0 is a parameter describing the ground roughness.

The selected target coherence is Davenport's coherence [22]:

$$\gamma(\xi,\omega)=\exp\left[-\frac{\lambda\omega\xi}{2\pi U(z)}\right] \tag{20}$$

with parameter $\lambda=10$ [22]. Then, the non-Gaussian target frequency–wavenumber spectrum (FKS) can be computed from:

$$S_{NG}^{T}(\omega,\kappa)=\frac{1}{2\pi}\int_{-\infty}^{\infty}S_{NG}(\omega)\,\gamma(\xi,\omega)e^{i\kappa\xi}d\xi \tag{21}$$

Substituting Eqs. (18) and (20) into Eq. (21) leads to:

$$S_{NG}^{T}(\omega,\kappa)=\frac{1}{2}\frac{200}{2\pi}u_*^2\frac{z}{U(z)}\frac{1}{\left[1+50\frac{\omega z}{2\pi U(z)}\right]^{5/3}}\left[\frac{1}{2\pi}\int_{-\infty}^{\infty}e^{-\lambda\omega\xi/2\pi U(z)}e^{i\kappa\xi}d\xi\right] \tag{22}$$

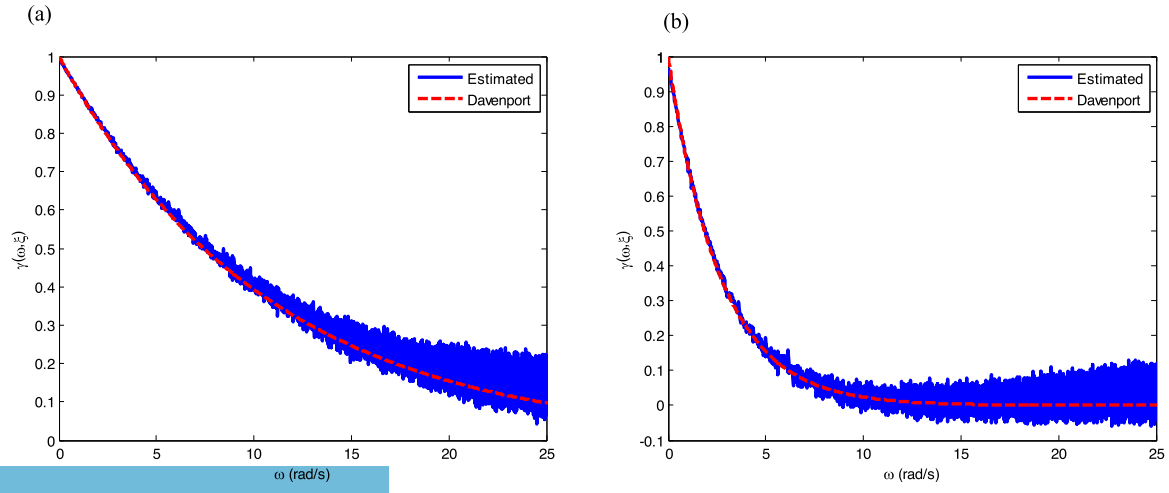

Fig. 4. Comparison of estimated coherences from 5000 generated non-Gaussian samples and corresponding target Davenport coherences: (a) $\gamma(\omega,\xi=2.34\ \text{m})$, (b) $\gamma(\omega,\xi=9.37\ \text{m})$.

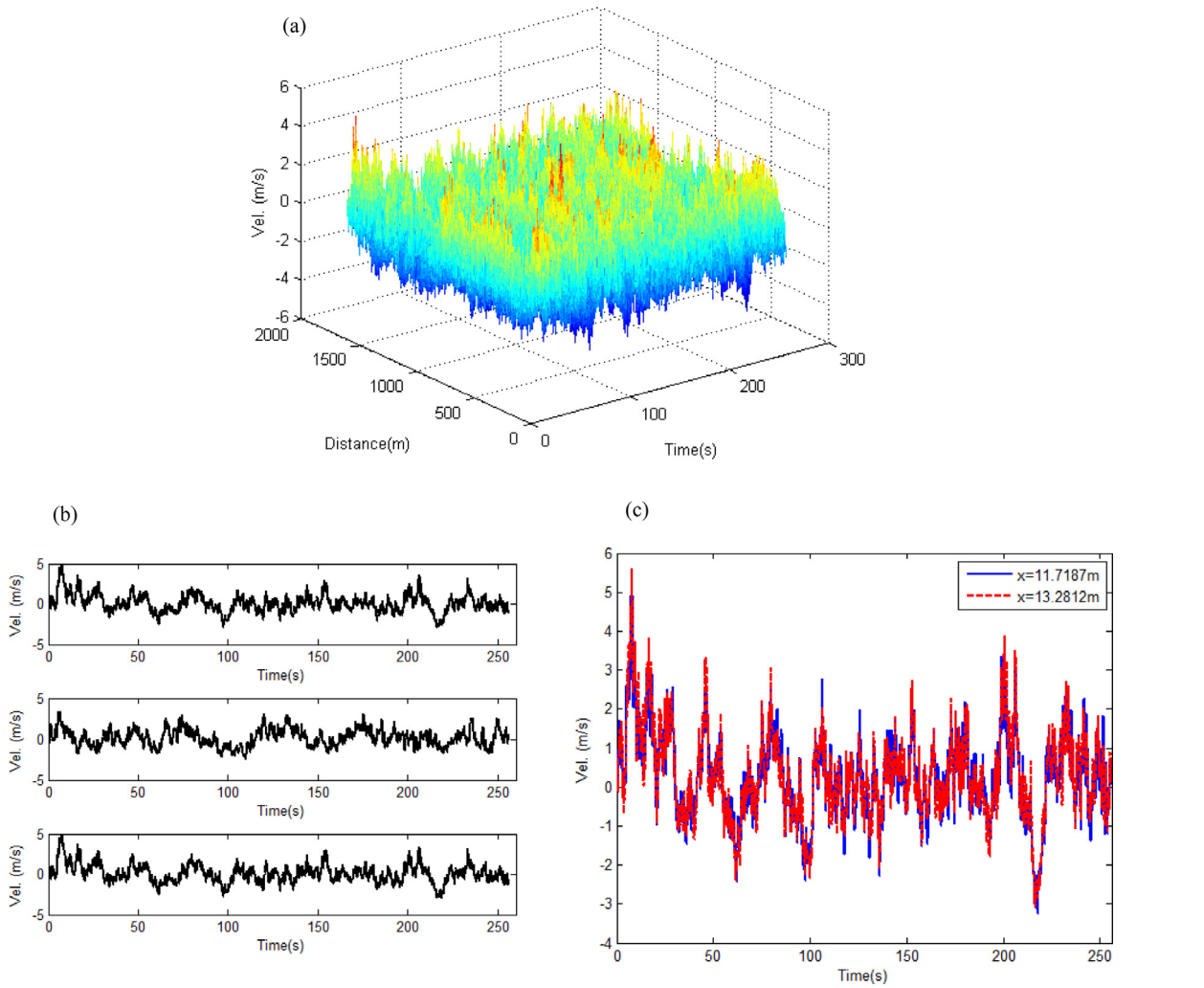

Fig. 5. Generated sample realization of wind velocity fluctuations modeled as a non-Gaussian stochastic wave: (a) Entire sample wave in space–time, (b) Selected time histories: top: $x = 0$ m, middle: $x = 800$ m, bottom: $x = 1600$ m, (c) Spatial coherency between neighboring points.

The integral in the above equation has an analytical solution, and Eq. (22) simplifies to:

$$S_{NG}^{T}(\omega,\kappa) = \frac{1}{2}\frac{200}{2\pi}u_*^2\frac{z}{U(z)}\frac{1}{\left[1+50\frac{\omega z}{2\pi U(z)}\right]^{5/3}}\left[\frac{\left(\frac{\lambda\omega}{\pi U(z)}\right)}{\kappa^2+\left(\frac{\lambda\omega}{2\pi U(z)}\right)^2}\right] \tag{23}$$

5.1. Problem parameter definitions

A bridge with an $L = 1600$ m main span is considered. The other parameters involved in the problem are set equal to:

$z = 50\,\text{m}; \quad z_0 = 0.03\,\text{m}; \quad U(z) = 40\,\text{m/s}$

The frequency–wavenumber discretization used is described by:

$$\omega_u = 8\pi\,\text{rad/s};\ N_\omega = 1024;\ \Delta\omega = \frac{\omega_u}{N_\omega - 1} = 0.0246\,\text{rad/s}$$

$$\kappa_u = \frac{2\left(N_\kappa - 1\right)}{L}\pi = 8.0385\,\text{m}^{-1};\ N_\kappa = 2048;\ \Delta\kappa = \frac{2\pi}{L} = 0.00393\,\text{m}^{-1}$$

Time and space are discretized as follows:

$$N_t = 2N_\omega = 2048;\ T = \frac{2\pi}{\Delta\omega} = 255.75\ \text{s};\ \Delta t = \frac{T}{N_t} = \frac{(2\pi/\Delta\omega)}{N_t} = 0.125\,\text{s};$$

$$N_x = 2N_\kappa = 4096;\ \Delta x = \frac{L}{N_x} = 0.391\,\text{m}$$

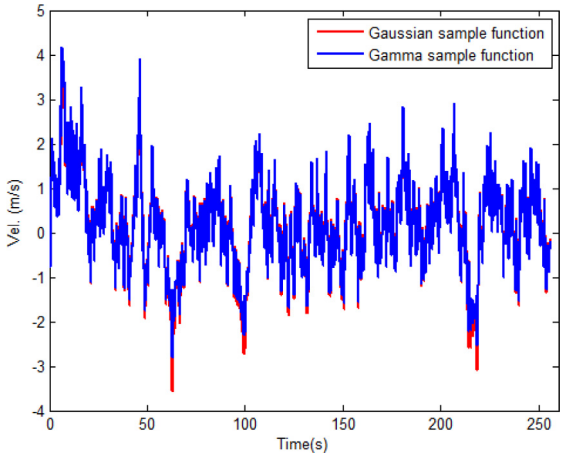

Fig. 6. Generated wind velocity fluctuation time histories at location $x = 38.67$m: underlying Gaussian and corresponding translated non-Gaussian (Gamma) time histories.

The above discretizations indicate that the velocity time histories will be computed at 4096 equidistant points along the length of the bridge's main span. The corresponding space interval is 0.391 m. Each

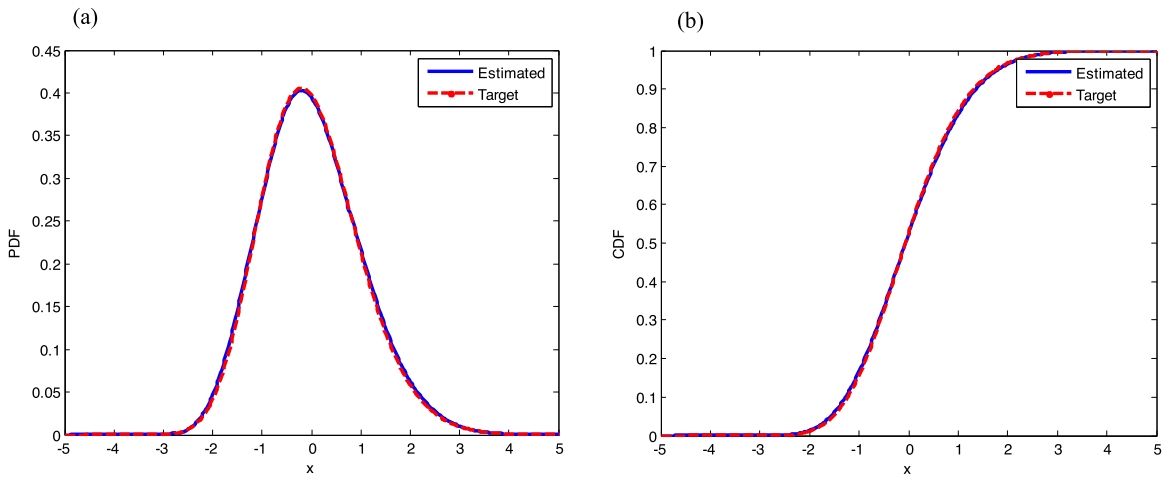

Fig. 7. Comparison of prescribed Gamma distribution to distribution estimated from one sample function: (a) PDF's, (b) CDF's.

of the 4096 time histories will be computed at 2048 equidistant time instants with a time interval of 0.125 s. It is clear that the currently existing approaches based on modeling the velocity time histories as a stochastic vector process (multi-variate stochastic process) would never be able to simulate time histories at such a large number of spatial locations/time instants.

5.2. Simulation results

The Gaussian FKS $S_G(\omega,\kappa)$ and non-Gaussian FKS $S_{NG}(\omega,\kappa)$ at the end of the iterative process described in Section 4 are shown in Figs. 2(a) and 2(b), respectively. Figs. 2(c) and 2(d) show the corresponding ensemble FKS computed from 5000 generated Gaussian and non-Gaussian sample functions, respectively. Fig. 2(e) displays the prescribed target FKS $S^T_{NG}(\omega,\kappa)$. There are minor differences between Fig. 2(a) and (b) as the selected Gamma distribution in Eqs. (16) and (17) is only mildly non-Gaussian. As expected, Fig. 2(a) is identical to Fig. 2(c), and Fig. 2(d) is converging to Fig. 2(b). Fig. 3 displays the FKS of just one generated non-Gaussian sample function. The convergence of the ensemble FKS of non-Gaussian samples from one sample to 5000 samples can be observed by comparing Figs. 3 to 2(d).

Using the 5000 generated non-Gaussian samples, two representative coherence functions are estimated at two different separation distances and plotted versus the corresponding target Davenport coherences in Fig. 4. For both selected separation distances, the match is very good as can be seen in Fig. 4.

A sample realization of the simulated non-Gaussian wave modeling wind velocity fluctuations is shown in Fig. 5. Fig. 5(a) shows the entire wave sample in space and time. Fig. 5(b) displays the corresponding time histories at $x = 0$ m, $x = 800$ m, and $x = 1600$ m. The time histories at $x = 0$ m and $x = 1600$ m display a high level of coherency because of the periodicity property of the spectral representation method. In contrast, the time history at $x = 800$ m shows no coherency to the time histories at $x = 0$ m and $x = 1600$ m because of the large separation distances. Finally, Fig. 5(c) shows corresponding superimposed and zoomed-in time histories at $x = 11.72$ m and $x = 13.28$ m to visually demonstrate the spatial coherency between neighboring points in space.

In Fig. 6, a generated Gaussian wind velocity time history at location x = 38.67 m along the length of the bridge is contrasted to the corresponding translated non-Gaussian (Gamma) time history. Although the Gamma PDF is only slightly non-Gaussian, it is clear that there are differences in the peaks of the two velocity time histories.

Fig. 7 displays the prescribed Gamma distribution and the estimated distribution computed from one generated sample function involving 4096 × 2048 data points. It is clear that the matching is excellent.

Finally, the CPU time necessary to generate one Gaussian sample function (4096 × 2048 data points) is 2 s, and then mapping it to the corresponding non-Gaussian Gamma sample function (4096 × 2048 data points) takes an additional 33 s. These CPU times were computed using 64-bit MATLAB R2014a on a desktop work-station with an Intel(R) Core(TM) i7-7700 processor and 24 GB of RAM. The capabilities of the proposed methodology become obvious when compared to existing methodologies based on modeling the velocity time histories as a stochastic vector process (multi-variate stochastic process). The existing vector process based methodologies are simply not capable of generating time histories at such a large number of spatial locations/time instants. The proposed stochastic wave based methodology is capable of doing so with great computational efficiency.

6. Conclusions

A methodology is proposed to simulate a non-Gaussian wind velocity field along the length of long-span bridges. In contrast to existing methodologies where these wind velocities are modeled as stochastic vector processes, the wind velocity field is modeled as a stochastic wave, continuous in space and time. This allows for simulation of wind velocity time histories at a virtually infinite number of points in space and time.

Acknowledgments

The first author H. Zhou received financial support from the National Natural Science Foundation of China (Grant Nos. 51578336 & 51108269) and the China Scholarship Council (No. 201608440509).

References

[1] M. Shinozuka, C.M. Jan, Digital simulation of random processes and its applications, J. Sound Vib. 25 (1972) 111–128.
[2] E. Simiu, R.H. Scanlan, Wind Effects on Structures, John Wiley, 1978.
[3] G. Deodatis, Simulation of ergodic multivariate stochastic processes, J. Eng. Mech. 122 (1996) 778–787.
[4] M.D. Di Paola, Digital simulation of wind field velocity, J. Wind Eng. Ind. Aerodyn. 74–76 (1998) 91–109.
[5] M.D. Di Paola, I. Gullo, Digital generation of multivariate wind field processes, Probab. Eng. Mech. 16 (2001) 1–10.
[6] A. Kareem, X. Chen, Proper orthogonal decomposition-based modeling analysis, and simulation of dynamic wind load effects on structures, J. Eng. Mech. 131 (2005) 325–339.
[7] W.W. Yang, T.Y.P. Chang, C.C. Chang, An efficient wind field simulation technique for bridges, J. Wind Eng. Ind. Aerodyn. 67 (1997) 697–708.
[8] Y. Cao, H. Xiang, Y. Zhou, Simulation of stochastic wind velocity field on long-span bridges, J. Eng. Mech. 126 (2000) 1–6.
[9] Y. Li, H. Liao, S. Qiang, Simplifying the simulation of stochastic wind velocity fields for long cable-stayed bridges, Comput. Struct. 82 (2004) 1591–1598.

[10] Y. Cao, Y. Wu, D. Li, H. Liu, N. Zhang, An improved approximation for the spectral representation method in the simulation of spatially varying ground motions, Probab. Eng. Mech. 29 (2012) 7–15.
[11] B. Benowitz, G. Deodatis, Simulation of wind velocities on long span structures: A novel stochastic wave based model, Proc. ICOSSAR 2013 (2013) 5549–5553.
[12] B. Benowitz, G. Deodatis, Simulation of wind velocities on long span structures: A novel stochastic wave based model, J. WEIA 147 (2015) 154–163.
[13] L. Peng, G. Huang, A. Kareem, Y. Li, An efficient space–time based simulation approach of wind velocity field with embedded conditional interpolation for unevenly spaced locations, Probab. Eng. Mech. 43 (2016) 156–168.
[14] L. Peng, G. Huang, X. Chen, A. Kareem, Simulation of multivariate nonstationary random processes: Hybrid stochastic wave and proper orthogonal decomposition approach, J. Eng. Mech. 143 (9) (2017) 04017064.
[15] Y. Song, J. Chen, Y. Peng, P.D. Spanos, J. Li, Simulation of nonhomogeneous fluctuating wind speed field in two-spatial dimensions via an evolutionary wavenumber-frequency joint power spectrum, J. WEIA (2018).
[16] M. Grigoriu, Crossings of non-Gaussian translation processes, J. Eng. Mech. 110 (1984) 610–620.
[17] M. Grigoriu, Applied Non-Gaussian Processes, Prentice Hall, 1995.
[18] M.D. Shields, G. Deodatis, P. Bocchini, A simple and efficient methodology to approximate a general non-Gaussian stationary stochastic process by a translation process, Probab. Eng. Mech. 26 (2011) 511–519.
[19] G. Deodatis, R.C. Micaletti, Simulation of highly skewed non-Gaussian stochastic processes, J. Eng. Mech. 127 (2001) 1284–1295.
[20] D.K. Kwon, A. Kareem, Peak factor for non-Gaussian load effects revisited, J. Struct. Eng. 137 (2011) 1611–1619.
[21] J.C. Kaimal, J.C. Wyngaard, Y. Izumi, O.R. Coté, Spectral characteristics of surface-layer turbulence, Q. J. R. Meteorol. Soc. 98 (1972) 563–589.
[22] A.G. Davenport, The dependence of wind loads on meteorological parameters, Wind Eff. Build. Struct. 1 (1967) 19–82.